The electronic structure of gadolinium grown on Mo(112)

1997 J. Phys.: Condens. Matter 9 10615

(http://iopscience.iop.org/0953-8984/9/48/007)

J. Phys.: Condens. Matter **9** (1997) 10615–10638. Printed in the UK PII: S0953-8984(97)80138-5

The electronic structure of gadolinium grown on Mo(112)

Carlo Waldfried, D N McIlroy† and P A Dowben

Department of Physics and Astronomy and the Center for Materials Research and Development, University of Nebraska–Lincoln, Lincoln, NE 68588-0111, USA

Received 6 December 1996, in final form 7 July 1997

Abstract. The electronic structure of strained ultra-thin and thin films of Gd grown on a corrugated Mo(112) surface are described. Gadolinium overlayers order at a coverage of $\frac{2}{3}$ monolayers forming a p(3 × 2) LEED pattern. At this coverage an interface state of b_1 symmetry (d_{xz}, p_x) is formed at a binding energy of ∼0.3 eV at the surface Brillouin zone centre ($\bar{\Gamma}$). The effective mass of this interface state was determined to be $(2.7 \pm 0.2)\ m_e$, in both orthogonal directions along the nearly square reduced Brillouin zone. For thicker Gd films of approximately 3 to 10 ML thickness, the corresponding gadolinium state switches symmetry to the a_1 representation (Gd $5d_{z^2-r^2}$ or 6s character) and has a much larger effective mass. The overlayer forms a rectangular surface Brillouin zone resembling the hcp (10$\underline{1}$2) surface. Gadolinium films thicker than approximately 10 ML form strained hexagonal ordered films also with substantial misfit dislocations. The strain of the thin hexagonal ordered Gd films is reflected by a reduced Brillouin zone size along $\overline{\Gamma\Sigma M}$ by approximately 4% with respect to the less strained Gd overlayers on W(110) and Gd(0001) single crystals. The induced strain severely alters the band structure of the Gd 5d/6s bulk bands, which disperse in the opposite direction relative to the corresponding bands of the relaxed Gd(0001) structure. The surface of the strained hexagonal fcc (111) or hcp (0001) Gd films forms a localized state of a_1 symmetry (Gd $5d_{z^2-r^2}$ or 6s character) at approximately 0.7 eV binding energy. There is little observed strain relief within the Gd films up to approximately 150 Å film thickness.

1. Introduction

Gadolinium is often used to typify the local moment elemental ferromagnet, based on the simplicity of the half filled 4f shell ($4f^7 5d^1 6s^2$). This results, in principle, in a completely polarized ground state, with a large magnetic moment of over 7 μ_B. Since the two most important elements of magnetism, magnetic moment and exchange splitting, are determined by the electronic structure, extensive work has been undertaken, both experimental [1–12] and theoretical [4, 13–22], to examine the electronic structure of hexagonal close packed (hcp) Gd(0001). The efforts made in investigating rare earth magnetism have belied the apparent simplicity of this system and many questions remain unexplained. In particular, the Gd(0001) exhibits very different magnetic ordering and electronic structure at the surface as compared to the bulk [5, 8, 9, 23–28]. This could be a result of electron localization of the Gd 5d, 6s bands [10, 15].

There are two approaches to generalizing the study of gadolinium surfaces in order to obtain a better understanding of rare earth magnetism. One way is to investigate surfaces other than the basal plane (0001). Since the electronic structure is expected to be different

† Permanent address: The Department of Physics, Engineering and Physics Building, The University of Idaho, Moscow, ID 83844-0903, USA.

0953-8984/97/4810615+24$19.50

for different surfaces, so should be the magnetic order. The other approach would be to strain the lattice. To date experimental difficulties [1, 2] have resulted in a paucity of experimental research examining the electronic structure of strained rare earth surfaces. Only a few studies have been undertaken for prism faces and other non-basal faces of the rare earths [2]. Small amounts of strain were obtained for ultra-thin films of Gd(0001) grown on W(110) [29], but very few differences were observed in the electronic structure which could be attributed to strain [1]. Nonetheless, lattice expansions, or contractions, can significantly alter the electronic structure, as has been shown on modified crystalline 3d transition metal films [30, 31]. Some calculations exist for the strained electronic structure of Pr [32], and little change is expected in the magnetic ordering of strained gadolinium based on model calculations [33].

We have been able to overcome the experimental difficulties in growing severely altered lattices of Gd by growing Gd on Mo(112) [34]. In this paper we will discuss the significantly modified electronic structure of ordered ultra-thin and thin Gd films grown on a corrugated Mo(112) substrate. The experimental band structure was mapped using angle resolved ultra-violet photoemission spectroscopy (ARUPS) and inverse photoemission electron spectroscopy (IPES), while structural analysis was undertaken by low-energy electron diffraction (LEED).

2. Experimental details

The photoemission experiments were acquired with synchrotron radiation using the 6 m toroidal grating monochromator at the Synchrotron Radiation Center in Stoughton, WI and the U5U undulator beamline at the National Synchrotron Light Source (NSLS) in Brookhaven, NY. The UHV chambers were equipped with a hemispherical electron energy analyser with an angular acceptance of $\pm 1^\circ$ and a combined energy resolution of $\sim$150 meV or better. The base pressure was maintained in the 10^{-11} Torr range. Light polarization measurements in the photoemission spectra were undertaken by comparing a photon incident angle of 35° (s-polarized light) or 45° (s+p-polarized light) to 65° or 70° (p-polarized light). Both systems were also equipped with a low-energy electron diffraction (LEED) system for determining crystallographic order of the surface.

The inverse photoemission electron spectroscopy (IPES) and LEED studies were undertaken in a UHV chamber with a base pressure of 7×10^{-11} Torr. The IPES spectra were acquired in the isochromatic mode ($\hbar\omega = 9.4$ eV) with a Geiger–Müller tube that was filtered with an SrF_2 entrance window and operated with an I_2/He filling. An electron gun based on the Zipf design [35] with a BaO cathode was used for the low-energy electron source. The overall resolution of the IPES system was found to be better than 400 meV.

The sample temperature was monitored with a Re/W 5%–26% thermocouple with an accuracy of ± 5 K. The Mo(112) substrate was cleaned by repeated cycles of annealing in oxygen at 1500 K and flashing at 2300 K. The Mo(112) surface was determined to be clean when the characteristic well ordered (1×1) LEED pattern (figure 1) was observed as well as by the absence of carbon and oxygen features in photoemission.

Ultra-thin Gd films in the submonolayer range and thin Gd films of various thicknesses up to 150 Å were grown at approximately 300 K and 150 K, respectively, on the Mo(112) crystal by slow physical evaporation and deposition. The chamber pressures during deposition were less than 1.5×10^{-10} Torr. The Gd film thickness was monitored with a quartz-crystal oscillator that was calibrated by means of the Mo 4p and Gd 4f core level intensities in conjunction with the well defined Gd interface structure that is formed at a coverage of $\frac{2}{3}$ monolayer. The films were consequently annealed at approximately 650 K

(ultra-thin films) and 500 K (thin films) up to 800 K (thicker films) for 5 minutes to obtain maximum structural order. The cleanliness of the Gd films were determined by the absence of contamination features attributed to oxygen at ∼6 eV binding energy and hydrogen at ∼3.8 eV, as well from the surface state intensity near E_F.

3. Gadolinium film growth and overlayer structures

Based on the intensity changes of the Gd 4f and substrate Mo 4p core level intensities (figure 1) we have determined that gadolinium adsorbs initially in a layer-by-layer (van der Merwe) or possibly the Stranski–Krastanov growth mode on the corrugated surface of Mo(112). This figure shows a roughly exponential decay of the Mo 4p core level intensity (acquired with 70 eV photon energy) for increasing Gd overlayer coverages up to 9 ML. Over the same range of coverage, the Gd 4f core level intensity (acquired with 52 eV photon energy) steadily increases. Within experimental error, Gd coverage and thin-film thickness increase linearly with exposure. The fact that the Mo 4p core level intensity can be completely obscured, combined with the LEED observation that the substrate reflections can be completely suppressed, eliminates the possibility of island growth under our deposition conditions.

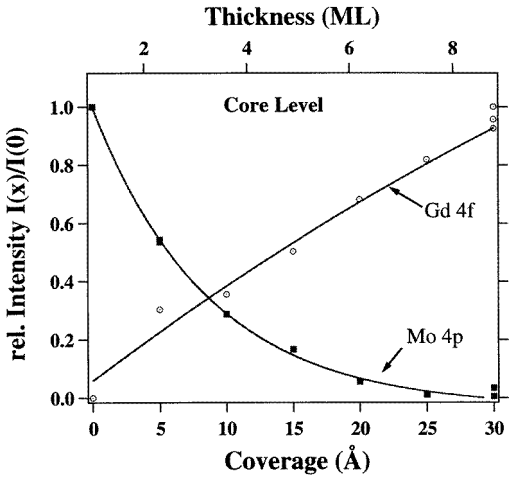

Figure 1. The relative Mo 4p (■) and Gd 4f (○), core level intensities as a function of film thickness in monolayers (top) and Å (bottom). The Mo 4p core levels were acquired with a photon energy of 70 eV, while the Gd 4f spectra were taken with a photon energy 52 eV.

The growth mode of gadolinium on the corrugated Mo(112) crystal surface was also studied with LEED, where the clean Mo(112) surface is characterized by a (1 × 1) LEED pattern (figure 2(a)). A model of the reciprocal lattice of the (112) surface is shown in figure 2(e). The surface Brillouin zone (SBZ) is rectangular in shape with zone dimensions of 1.15 $Å^{-1}$ along the $\overline{\Gamma X}$-direction and 0.706 $Å^{-1}$ along the $\overline{\Gamma Y}$-direction.

The deposition of submonolayer thin films of Gd results in a p(3 × 2) LEED pattern (figure 2(b)). These ultra-thin films attain maximum ordering for an annealing temperature of approximately 650 K and a film thickness of approximately 0.7 monolayers (ML). The reduced Brillouin zone of an ultra-thin Gd film with a coverage of a developed p(3 × 2) structure is shown in figure 2(f). The zone dimensions are 0.383 $Å^{-1}$ along the $\overline{\Gamma X}'$-

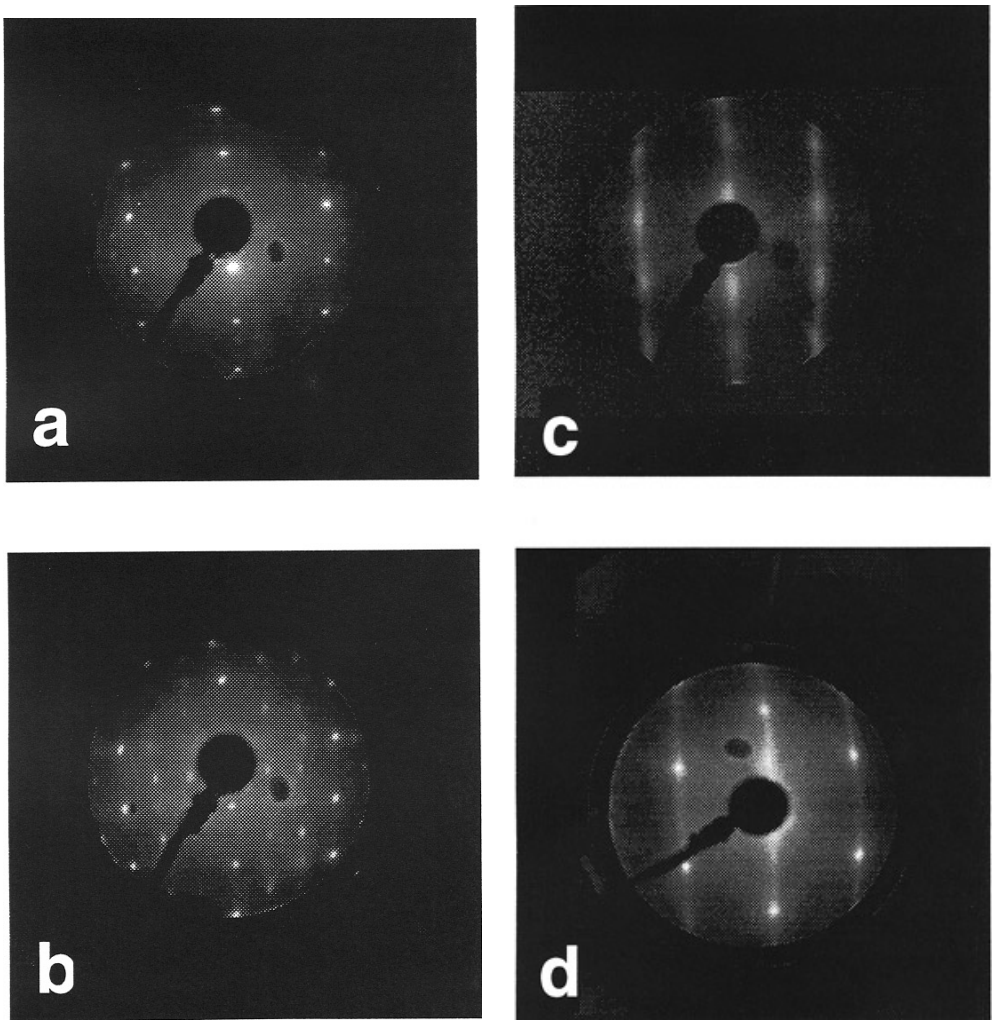

Figure 2. The LEED pictures of (a) a clean Mo(112) surface, (b) a 0.7 ML Gd film grown on the Mo(112) surface, (c) a 25 Å thick Gd film grown on Mo(112) and (d) a 50 Å thick Gd film grown on Mo(112). All films were annealed at 650 K, and acquired with an electron energy of 74.2 eV. The Brillouin zones of the LEED patterns (a)–(d) are displayed in panels (e)–(h). The (1 × 1) LEED structure of the clean Mo(112) substrate (a) implies a rectangular Brillouin zone with zone dimensions of 1.15 Å^{-1} along $\overline{\Gamma X}$ and 0.706 Å^{-1} along $\overline{\Gamma Y}$ (e). The ultra-thin Gd overlayer is reflected by a p(3 × 2) LEED pattern (b) which spans a nearly square reduced Brillouin zone ($\overline{\Gamma X}' = 0.38$ Å^{-1}, $\overline{\Gamma Y}' = 0.35$ Å^{-1}) (f). The thin Gd films reflect a rectangular Brillouin zone with zone dimensions of approximately 0.83 Å^{-1} along $\overline{\Gamma X}''$ and 0.72 Å^{-1} along $\overline{\Gamma Y}''$ (g). The surface Brillouin zone of the hexagonal ordered structure of the thicker Gd film (d) is displayed in panel (h). The streaks in the LEED pictures (c) and (d) are in the direction perpendicular to the substrate corrugations.

direction and 0.353 Å^{-1} along the $\overline{\Gamma Y}'$-direction, which form a nearly square Brillouin zone.

The modelled reciprocal space of the 0.7 ML thick Gd film is shown in figure 3(a), where the Mo substrate reciprocal lattice vectors are $\boldsymbol{a}_1^*$ and $\boldsymbol{a}_2^*$, and the principal reciprocal

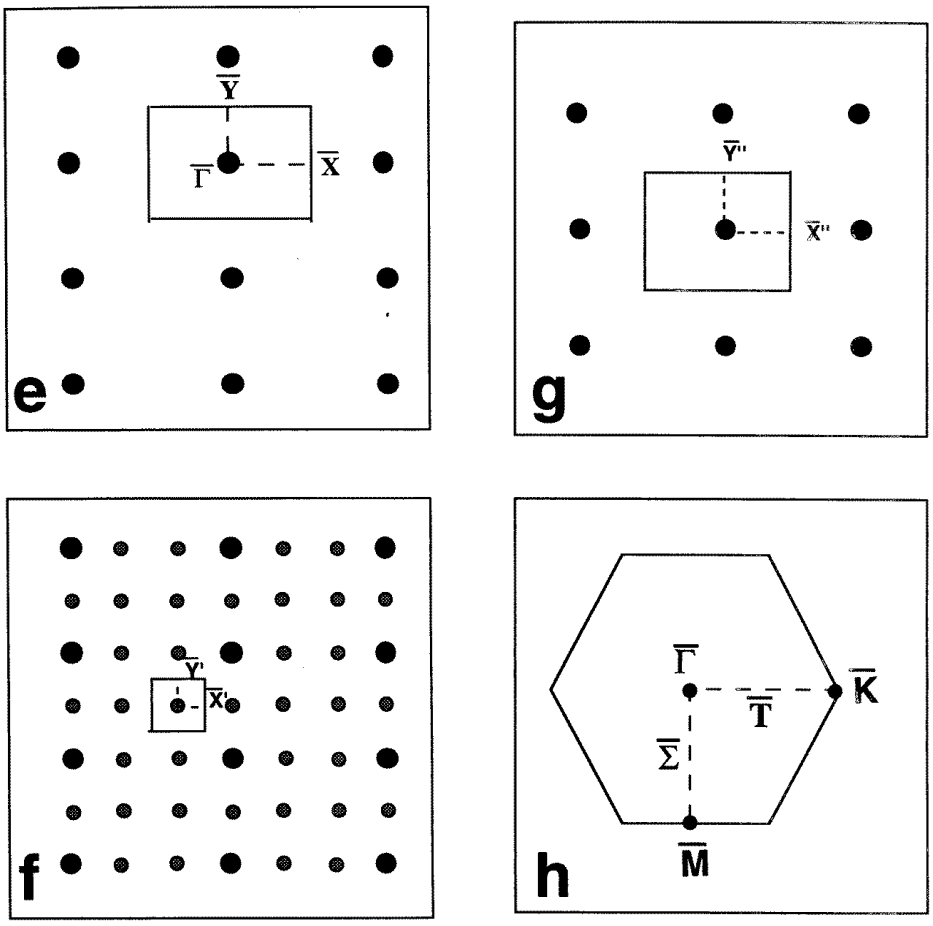

Figure 2. (Continued)

lattice vectors of the Gd overlayer are denoted by $\boldsymbol{b}_1^*$ and $\boldsymbol{b}_2^*$. The principal reciprocal lattice vectors are expressed in terms of $\boldsymbol{a}_1^*$ and $\boldsymbol{a}_2^*$ by the representation matrix $\tilde{\mathcal{G}}^{-1}$ as follows:

$$\begin{pmatrix} \boldsymbol{b}_1^* \\ \boldsymbol{b}_2^* \end{pmatrix} = \begin{pmatrix} \frac{2}{3} & \frac{1}{2} \\ \frac{2}{3} & -\frac{1}{2} \end{pmatrix} \begin{pmatrix} \boldsymbol{a}_1^* \\ \boldsymbol{a}_2^* \end{pmatrix}. \tag{1}$$

The real space primitive translation vectors are obtained through $\boldsymbol{b} = \mathcal{G}\boldsymbol{a}$, which is explicitly represented by

$$\begin{pmatrix} b_1 \\ b_2 \end{pmatrix} = \begin{pmatrix} \frac{3}{4} & 1 \\ \frac{3}{4} & -1 \end{pmatrix} \begin{pmatrix} a_1 \\ a_2 \end{pmatrix}. \tag{2}$$

The vectors that describe the primitive cell of the Gd overlayer lattice are consequently defined by: $\boldsymbol{b}_1 = (\frac{3}{4})\boldsymbol{a}_1 + \boldsymbol{a}_2$ and $\boldsymbol{b}_2 = (\frac{3}{4})\boldsymbol{a}_1 - \boldsymbol{a}_2$, which are indicated in figure 3. One possible model for the real space of the ultra-thin films of Gd is constructed by the two lattice vectors $\boldsymbol{b}_1$ and $\boldsymbol{b}_2$, and is shown in figure 3(b). In this model, the overlayer Gd lattice has been translated by $\frac{1}{2}$ of an Mo–Mo lattice distance ($(\frac{1}{2})\boldsymbol{a}_1$) in order to place the Gd atoms in the trough positions of the corrugated Mo(112) lattice. The distinct horizontal streaks

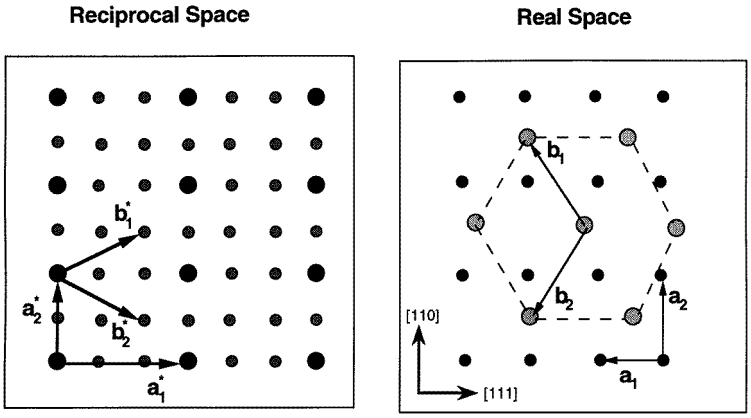

Figure 3. The reciprocal space lattice of a 0.7 ML Gd film grown on Mo(112) (left). The Mo substrate diffraction spots are represented by the large black circles, while additional Gd diffraction spots are indicated by smaller grey circles. The reciprocal lattice vectors for Mo are labelled $\boldsymbol{a}_1^*$ and $\boldsymbol{a}_2^*$. The principal lattice vectors for the Gd overlayer are indicated by $\boldsymbol{b}_1^*$ and $\boldsymbol{b}_2^*$. A model for the real space overlayer arrangement is shown in the right panel. Here, the small black circles represent the lattice sites of the Mo atoms, while large grey circles indicate the Gd positions. The lattice vectors are represented by $\boldsymbol{a}_1$ and $\boldsymbol{a}_2$ for Mo and $\boldsymbol{b}_1$ and $\boldsymbol{b}_2$ for Gd. The dotted lines are drawn to help the reader to identify the nearly hexagonal arrangement of the Gd overlayer.

in the pertinent LEED pattern (figure 2(b)) suggest that formation of domains occurs with translational shifts relative to the substrate lattice along the ⟨110⟩ crystallographic direction. This, to some extent, justifies our translational shift in the presented model for the ultra-thin Gd overlayer (figure 3(b)). We want to emphasize that our LEED data alone do not uniquely define the real space lattice positions of the Gd atoms. We cannot and did not determine the exact positions of the Gd atoms shown in figure 2(b) relative to the Mo(112) surface lattice and no specific translational vector can be identified. The coverage of an overlayer is determined by the determinant of the representation matrix $\tilde{\mathcal{G}}^{-1}$. Our choice of principal reciprocal lattice vectors $\boldsymbol{b}_1^*$ and $\boldsymbol{b}_2^*$ determines the film thickness as $\frac{2}{3}$ of a monolayer, which is in excellent agreement with the thickness of 0.7 ML, as determined by the calibrated thickness monitor, and the photoemission. The initial adsorption of Gd on the corrugated Mo(112) surface results in the development of an interface state at approximately 0.3 eV binding energy at $\bar{\Gamma}$, with maximum intensity at a coverage of approximately 0.7 ML (as discussed later).

The diamond-shaped Gd unit cell, which is constructed from the two lattice vectors $\boldsymbol{b}_1$ and $\boldsymbol{b}_2$, spans an overlayer lattice that resembles an anisotropic distorted hexagon with lattice constants of 4.59 Å and 4.89 Å (indicated by the dashed lines in figure 3(b)). These lattice constants are large compared to the lattice constant of 3.64 Å for hcp Gd [36] and represents an expansive strain of more than 25% for the monolayer film. The unfavourable lattice match between the furrowed Mo(112) substrate and the naturally hexagonal Gd film appears in a large and uniaxially expanded Gd hexagonal structure.

Thin films of gadolinium, several monolayers thick, grow in a rectangular structure that are ordered along the furrow direction (⟨111⟩ substrate direction) [34]. Perpendicular to the substrate corrugation lines the crystallographic order is destroyed. This is indicated by the vertical streaks of the rectangular LEED pattern in figure 2(c), of an 8 ML thick Gd

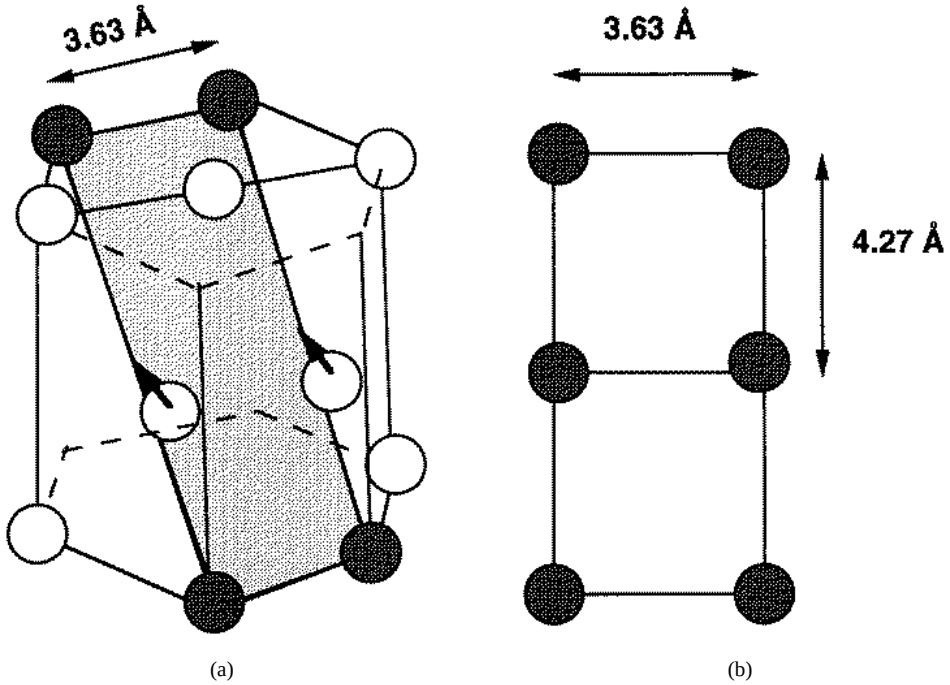

Figure 4. (a) The unit cell of a hexagonal closed packed (hcp) lattice. The shaded area indicates the (10$\underline{1}$2) plane. (b) The reconstructed (10$\underline{1}$2) plane for Gd as seen from the vacuum with lattice spacings of 3.63 Å and 4.27 Å.

film. The rectangular surface Brillouin zone for this thin Gd film is shown in figure 2(g). The zone dimensions are 0.84 Å^{-1} along the $\overline{\Gamma X}''$-direction and 0.73 Å^{-1} along the $\overline{\Gamma Y}''$-direction. These reciprocal lattice parameters represent approximately 25% uniaxial strain for the hcp (10$\underline{1}$0) surface and 18% uniaxial strain for the fcc (110) surface, but less than 4% strain for a reconstructed hcp (10$\underline{1}$2) surface (see figure 4). We have rectangular lattice parameters of 3.74 Å and 4.30 Å compared to the ideal 3.63 Å and 4.27 Å lattice constants. Epitaxial growth of tilted hcp (10$\underline{1}$2) planes of rare earth on bcc (112) substrates have also been reported by Du *et al* [37, 38]. The reconstructed hcp (10$\underline{1}$2) plane is thus a likely growth mode for the Gd films of intermediate thickness, although our measurements cannot uniquely define the lattice orientation.

Thicker Gd films of more than approximately 10 ML exhibit a streaked hexagonal LEED pattern as shown in figure 2(d). The hexagonal Brillouin zone is shown schematically in figure 2(h). Both hcp (0001) and fcc (111) structures are possible and not clearly distinguishable by our LEED studies. Careful analysis of LEED and thickness dependent experimental electronic structure mappings (as discussed later) both indicate that the thicker Gd films grown on Mo(112) are strained to a larger lattice spacing as compared to the relaxed Gd(0001) by approximately 4%. The strain is not relieved for film thicknesses of up to 150 Å. The absence of strain relief for the thicker films and the persistence of the modified electronic structure (discussed later) indicate that the thicker Gd films grow in a strained hcp (0001) or a strained fcc Gd(111) surface structure. The possibility of a fcc Gd(111) plane has also been addressed by theory [39], which suggests an unusual reduction of the spin moment of the surface layer as compared to the bulk.

4. The electronic structure of the submonolayer ultra-thin films

The coverage dependent normal emission photoemission spectra for gadolinium overlayers on Mo(112) are shown in figure 5 for coverages of 0 to 1.5 monolayers. The clean Mo(112) valence band is characterized by (i) a bulk band at 1.8 eV below E_F, (ii) a surface state at a binding energy of approximately 3.0 eV, (iii) a bulklike state near the Fermi level at 0.1 eV binding energy and (iv) a broad bulk band shoulder 4.3 eV below E_F [40]. With the adsorption of submonolayer coverages of Gd, the molybdenum surface state at 3.0 eV binding energy decreases rapidly and two new Gd-induced states at approximately 0.3 eV and 1.8 eV binding energy develop. This is seen clearly in figure 6 which shows the direct comparison between the 0.7 ML Gd film grown on Mo(112) and the clean Mo(112) surface.

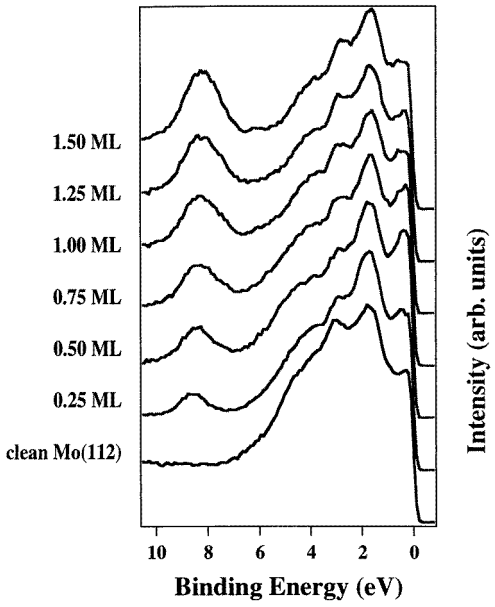

Figure 5. The normal emission valence-band spectra of ultra-thin films of Gd grown on Mo(112) for various coverages ranging from 0 to 1.5 ML. The spectra were acquired at a temperature of approximately 190 K, using a photon energy of 52 eV.

The weaker Gd feature at 1.8 eV below E_F is not easily seen in figures 5 and 6 because of overlapping Mo bulk bands. The existence of this state is however identified from the differences in the light polarization dependence with respect to the detection plane. Both the 0.3 eV and 1.8 eV Gd-induced bands have different symmetry as compared to the states of the clean Mo(112) surface with similar binding energies [41]. In addition, the two Gd-induced bands at 0.3 eV and 1.8 eV below E_F at $\bar{\Gamma}$ exhibit different polarization dependence (and therefore different symmetry) as seen in figure 7(a).

The Gd 4f core levels are at a binding energy of 8.3 eV and increase in intensity with increasing Gd coverage (see figure 1). This behaviour of the shallow core level is quite different from that observed for the Gd state near the Fermi energy. The intensity of the Gd induced valence state at 0.3 eV below E_F increases rapidly for small coverages and peaks at a coverage of approximately 0.7 ML. With Gd coverages greater than 0.7 ML the intensity of the Gd-induced state diminishes reaching a minimum at a coverages of 1.3 ML. Since

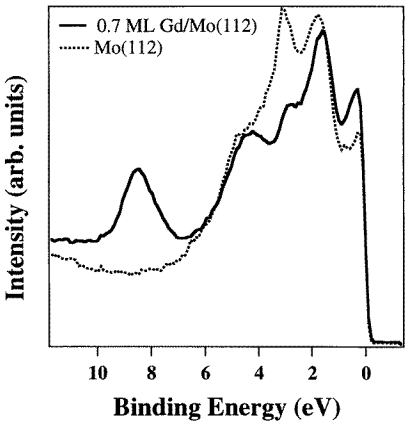

Figure 6. Two normal emission valence-band spectra for a clean Mo(112) surface (· · · · · ·) and a 0.7 ML ultra-thin Gd film grown on Mo(112) (——). Both spectra were acquired at 150 K with a photon energy of 52 eV.

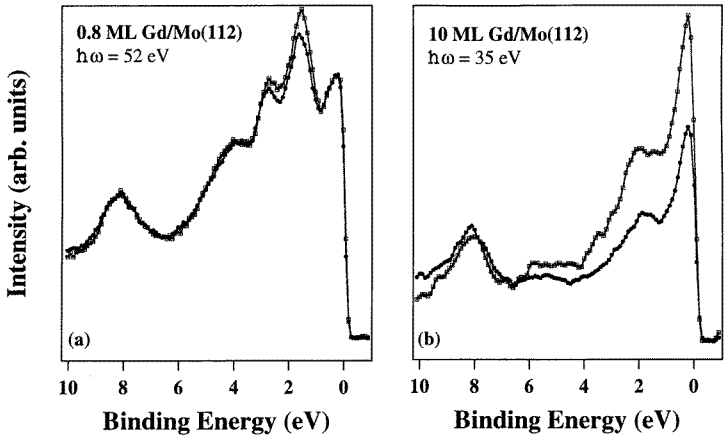

Figure 7. Normal emission photoemission spectra acquired with (s + p)-polarized light (●), and p-polarized light (□) for (a) a 0.8 ML Gd/Mo(112) film and (b) a 10 ML film.

this Gd-induced state is only present for a very narrow region of coverages, we identify this state as a Gd interface state. Both the Gd-induced interface state near E_F and the Gd state at 1.8 eV binding energy are highly susceptible to small amounts of contamination, such as oxygen. This is characteristic of a surface or interface state, in particular the Gd(0001) surface state [10, 41, 42]. These findings are demonstrated in figure 8 which shows a 0.7 ML thick Gd film which has been exposed to increasing amounts of oxygen, ranging from an exposure of 0.3 L to 1.1 L. Concomitant with the formation of the typical oxygen-induced features at 4.3 eV and approximately 6 eV binding energy [42, 43], the two Gd states at 0.3 eV and 1.8 eV below E_F are suppressed.

The ordering of the ultra-thin Gd films is always an important issue. Increased ordering could be obtained on annealing the ultra-thin Gd films, which resulted in the enhanced development of the Gd interface state. The effects of the film ordering are demonstrated in

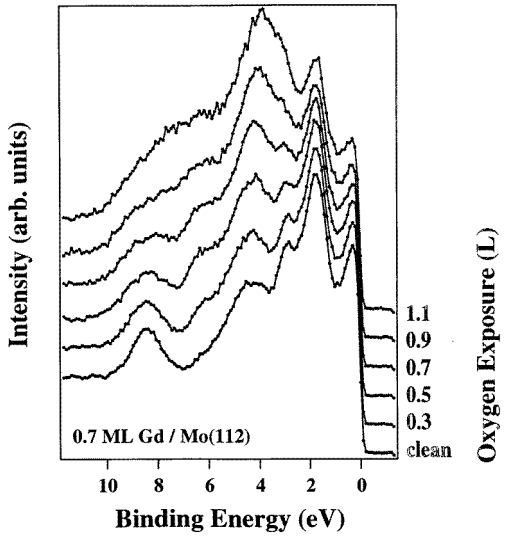

Figure 8. The normal emission valence-band spectra for a 0.7 ML Gd film grown on Mo(112) as a function of oxygen exposure. The spectra were acquired at 180 K with (s + p)-polarized light and a photon energy of 52 eV.

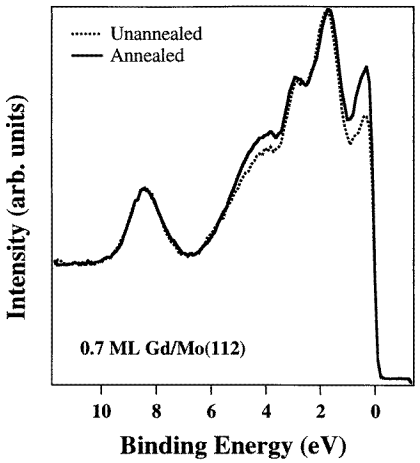

Figure 9. Two normal emission valence-band spectra for a 0.7 ML thick Gd overlayer on Mo(112) acquired at approximately 190 K with 52 eV photons. The dotted spectrum was collected for the film as is, while the solid line shows the same film annealed at 650 K for 5 minutes.

figure 9, which shows two spectra of a 0.7 ML Gd film, grown at room temperature (i) as deposited and (ii) annealed at 650 K for 5 minutes. The annealed spectrum results in a strong enhancement of the interface state intensity, while the remainder of the valence-band spectrum does not change.

With a well ordered film, band dispersion can be measured. We studied the dispersion of the Gd-induced interface state along the $\overline{\Gamma X'}$ and $\overline{\Gamma Y'}$ high-symmetry directions of the adsorbate-induced reduced Brillouin zone, which are along the ⟨111⟩ and ⟨110⟩ substrate

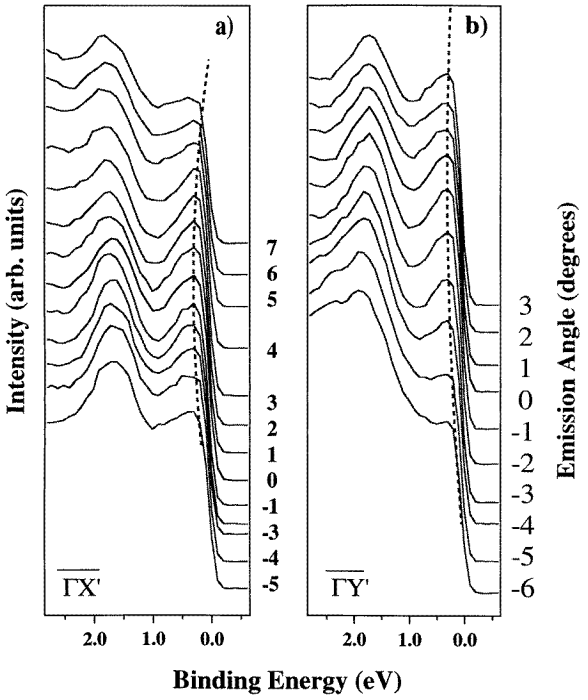

Figure 10. The angle dependent photoemission spectra of a 0.7 ML thick Gd film grown on Mo(112) along the $\overline{\Gamma X}'$ (top) and $\overline{\Gamma Y}'$ (bottom) high-symmetry directions of the reduced surface Brillouin zone. The spectra were acquired at 150 K with a photon energy of 52 eV. The dotted lines indicate the peak positions of the Gd interface state.

crystallographic directions, respectively. Figure 10 shows two sets of photoemission valence-band spectra of a 0.7 ML Gd film that have been acquired at various points along $\overline{\Gamma X}'$ (top) and $\overline{\Gamma Y}'$ (bottom). The Gd-induced interface state at 0.3 eV at $\bar{\Gamma}$ disperses parabolically towards the Fermi level for both directions, as indicated by the dotted lines. The dispersion $E(k_{\|})$ for the Gd-induced interface state is shown in figure 11. This figure includes data points for the dispersion along $\overline{\Gamma X}'$ (●), (top), as well as along $\overline{\Gamma Y}'$ (▲) (bottom), where the error bars indicate the uncertainty in the binding energies. The reduced Brillouin zone of the Gd interface state is indicated by vertical bars marking the zone edges $\bar{X}'$ and $\bar{Y}'$ at 0.35 Å^{-1} and 0.38 Å^{-1}, respectively. The data points along both high-symmetry directions indicate nearly overlapping dispersive behaviour and were fitted with a parabolic curve to determine the effective mass according to:

$$\frac{1}{m^*} = \frac{1}{\hbar}\frac{\partial^2 E}{\partial k^2}. \tag{3}$$

An average value of $m^* = (2.7 \pm 0.2)\ m_e$ was obtained from the line shape fitting of our experimental data (figure 11).

The crossing of the Fermi level by the light-effective-mass Gd-induced interface state at the zone edge has been independently confirmed with inverse photoemission. Figure 12(a) shows two inverse photoemission spectra acquired at approximately 200 K with the electrons incident at an angle of 16 degrees relative to the surface normal along $\overline{\Gamma X}'$, one for a clean Mo(112) surface and a second for a 0.7 monolayer Gd film grown on Mo(112). The

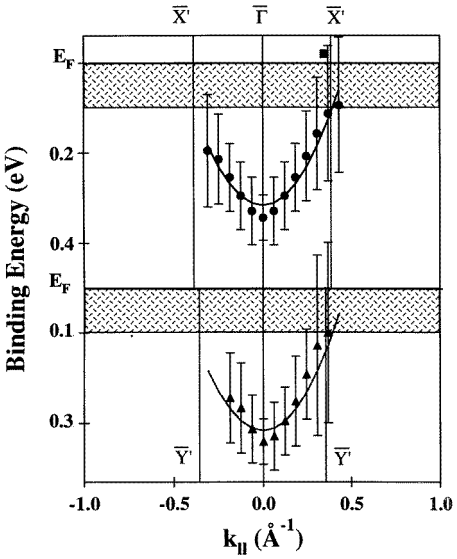

Figure 11. The band dispersion of the Gd interface state of a 0.7 ML thick Gd film grown on Mo(112). The figure includes data points obtained from the dispersion along the $\overline{\Gamma X}'$ high-symmetry line (●) (top panel), and along the $\overline{\Gamma Y}'$ high-symmetry line (▲) (bottom panel). The error bars indicate the uncertainty in the binding energy positions along both directions. The data points were fitted with a parabolic function, centred at $\bar{\Gamma}$, which is shown as a solid line. The in-plane momentum of the Fermi level crossing of the interface state as determined by inverse photoemission is indicated by a filled box. The shaded areas represent the limit in resolution near the Fermi level.

unoccupied density of states of the Gd-covered surface, derived from difference spectra, exhibits a significant increase in intensity in the vicinity of the Fermi level as compared to the clean Mo(112) surface. The angular dependence along $\overline{\Gamma X}'$ of the density of states near the Fermi level of a 0.7 ML Gd film grown on Mo(112) is displayed in figure 12(b). The unoccupied density of states clearly shows a variation in intensity in the region next to the Fermi level with the maximum being found for an electron incidence angle of approximately 16°–17°. This indicates the Fermi level crossing of the Gd-induced interface state for a parallel wave vector component of (0.35 ± 0.025) Å^{-1}, which is also indicated as a solid box in the top panel of figure 11. The Fermi level crossing occurs at a different wave vector from the Mo(112) surface resonance band along $\overline{\Gamma X}$ [44].

The overall symmetry of the reduced SBZ of the ultra-thin Gd film is represented by the C_{2v} symmetry group. The Gd interface state near the Fermi level appears with nearly equal photoelectron emission intensity in PES for (s + p)-polarized as well as p-polarized light, which is shown in figure 7(a). This suggests a symmetry assignment for the interface state of b_1 (Σ_3 in the bulk representation) or b_2 (Σ_4) representation. The Gd-induced surface state at 1.8 eV binding energy, in contrast, is strongly enhanced with p-polarized light. In the C_{2v} symmetry group at $\bar{\Gamma}$, this is only possible for a state with a_1 (Σ_1) symmetry representation. This limits the possible character for the 1.8 eV state to predominantly Gd $6s/5d_{z^2-r^2}$ rectangular representations.

The Gd-induced state at 0.3 eV binding energy at $\bar{\Gamma}$ disperses upwards toward the Fermi level along both high-symmetry lines $\overline{\Gamma X}'$ and $\overline{\Gamma Y}'$. This indicates a bonding situation at the zone centre and antibonding character at the zone boundaries. The bonding configuration

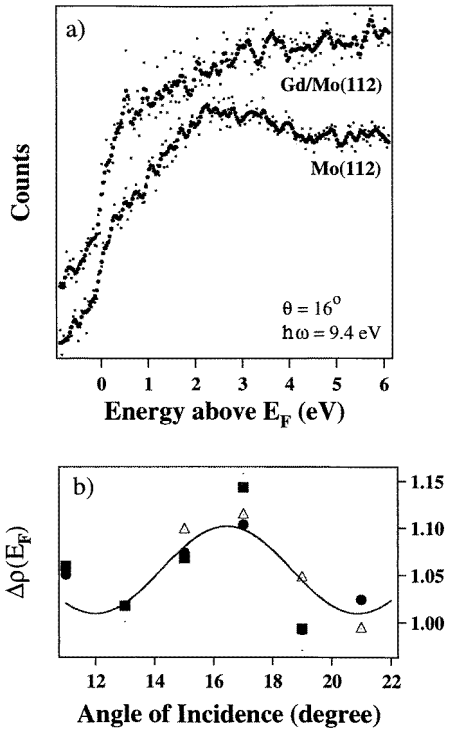

Figure 12. (a) Inverse photoemission spectra acquired for a clean Mo(112) surface and a 0.7 ML Gd film grown on Mo(112). The spectra were taken at approximately 200 K at an electron incident angle of 16 degrees. (b) The relative integrated density of states near the Fermi level as a function of electron incidence angle for a 0.7 ML Gd film grown on Mo(112). The data points represent a collection from several independently grown ultra-thin films, as indicated by different symbols.

at $\bar{\Gamma}$ is such that the Gd $5d_{xz}/6p_x$ orbitals are strongly hybridized with the Mo $4d_{xz}/5p_x$ orbitals. The second Gd-induced valence-band feature at 1.8 eV binding energy which is of a_1 symmetry can only be filled by Gd $6s/5d_{z^2-r^2}$ electrons that hybridize with Mo $4d_{z^2-r^2}/5p_z$ orbitals. These two bands are consistent with electron counting (of the $4f^7 5d^1 6s^2$ configuration of Gd). This symmetry assignment rules out certain bonding sites of the Gd interface atoms at the Mo(112) surface, for example, atop sites or row bridge sites. In order to satisfy the determined bonding symmetry the Gd atoms have to occupy bonding sites in the Mo(112) troughs. The two possible bonding sites are either at the cross hollows, or the trough bridge sites. The bonding symmetry assignments strongly support the lattice model in figure 3(b).

With the completion of the Gd–Mo interface all the valence electrons of the system are used for hybridization and bonding. There are no additional free electrons present, which makes the Gd/Mo(112) interface layer system a fairly inert system. This is strongly supported by our observation that the ultra-thin Gd film is far less reactive to adsorbates than expected.

Above $\frac{2}{3}$ ML coverage there is a transition to a new electronic structure, associated with the Gd overlayer. The hexagonal overlayer of Gd films one atom thick is replaced

by Gd atoms adopting a rectangular unit cell resembling hcp (10$\underline{1}$2). Accompanying the decline of the interface state near the Fermi level with increasing coverage beyond $\frac{2}{3}$ ML the spectral intensity of a feature at approximately 3.0 eV binding energy increases (see figure 5), attributable to another Gd-induced state.

5. The electronic structure of thin Gd films

The intermediate-thickness films, 3 ML $< \Theta <$ 10 ML, adopt a Brillouin zone different from the hexagonal structure formed by gadolinium at higher coverages as well as the hexagonal overlayer structure for lower coverages. The band structure is that of a much strained film. Two sets of photoemission valence-band spectra of thin gadolinium films, approximately 25 Å thick (10 ML), are shown in figure 13 for (s + p)-polarized light and a photon energy of 35 eV. The spectra were recorded at various points along the high-symmetry lines $\overline{\Gamma X}''$ (top), and $\overline{\Gamma Y}''$ (bottom) of the rectangular surface Brillouin zone, which are along the ⟨111⟩ and ⟨110⟩ crystallographic directions of the substrate or ⟨10$\underline{1}$0⟩ and ⟨0$\underline{1}$12⟩ directions of hcp (10$\underline{1}$2), respectively. The normal emission spectra are characterized by the Gd 4f core level at 8.4 eV binding energy, the Gd 5d, 6s bulk band at ∼1.8 eV below E_F and the relatively sharp and narrow surface state Gd $5d_{z^2-r^2}$ surface state at ∼0.3 eV binding energy. We have established the symmetry of this latter state from the light polarization dependence. Figure 7(b) shows two normal emission valence-band spectra in (s + p)- and p-polarized light for an approximately 10 ML thick Gd film. For the intermediate-thickness Gd films with rectangular Brillouin zone, both the surface state at 0.3 eV binding energy and the bulk bands at 1.8 eV below E_F are strongly enhanced under p-polarized light. This indicates that both bulk and surface have a_1 symmetry, i.e. Gd $5d_{z^2-r^2}$/Gd 6s character.

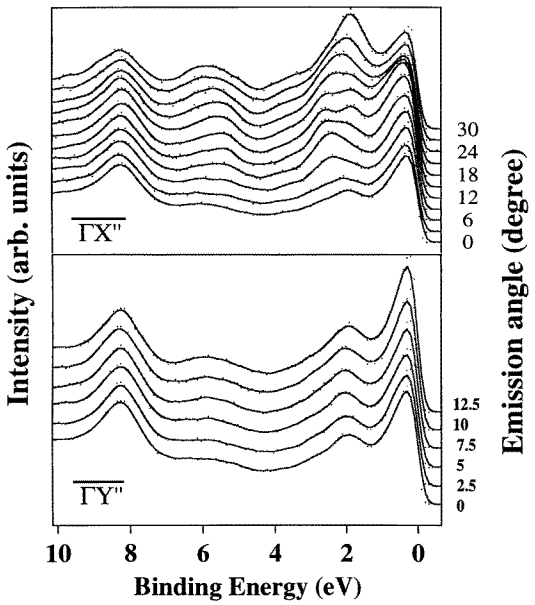

Figure 13. The emission angle dependent photoemission spectra of a 25 Å Gd film grown on Mo(112) along the $\overline{\Gamma X}''$ (top) and $\overline{\Gamma Y}''$ (bottom) high-symmetry directions of the surface Brillouin zone. The spectra were acquired at 150 K with a photon energy of 35 eV.

At normal emission the valence-band spectrum of the thin rectangular ordered Gd film very closely resembles the photoemission spectrum of the Gd(0001) [5, 8, 9], with the exception of the markedly broader state in the vicinity of the Fermi energy. A sharp surface state feature with high photoelectron emission intensity is characteristic of a hexagonal ordered Gd (0001) surface [5, 8, 9]. Both the 5d, 6s bulk bands and the surface state of the dislocated and rectangular ordered films exhibit pronounced band dispersion along the $\overline{\Gamma X}''$ direction of the SBZ. In contrast, along the $\overline{\Gamma Y}''$ direction, the Gd 5d, 6s bulk bands are dispersionless within the resolution of the analyser. The electronic valence-band structure along the $\overline{\Gamma X}''$ high-symmetry line is shown in figure 14 for 20–25 Å thick films of Gd. The dislocations and defects in the crystal structure of thin Gd films (thickness of 3–10 ML) are reflected by streaks in the rectangular LEED pattern which are oriented along the ⟨110⟩ direction. This indicates long-range order along the substrate corrugation direction (⟨111⟩ direction), with the dislocations predominantly in the direction perpendicular to the Mo(112) furrows (along the ⟨110⟩ direction). This is supported by the dispersion of the thin Gd films grown on Mo(112). There is no dispersion along the $\overline{\Gamma Y}''$ direction of the SBZ (figure 13), which is the direction perpendicular to the substrate corrugation lines, but strong band dispersion of both the bulk bands ($\Delta E = 0.8$ eV) and surface state ($\Delta E = 0.2$ eV), along the $\overline{\Gamma X}''$ high symmetry line (parallel to the corrugation). The absence of dispersion along the $\overline{\Gamma Y}''$ direction is characteristic of the failure of long-range order and deficiency in lattice periodicity.

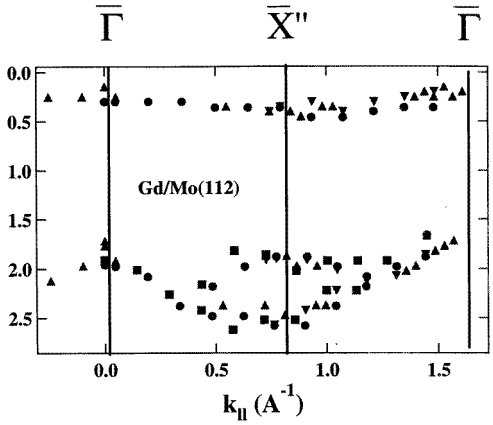

Figure 14. The band dispersion of thin Gd films along the $\overline{\Gamma X}''$ direction of the Brillouin zone. The figure was constructed from data acquired from films of 20 Å nominal thickness for several independently grown films (different symbols).

The differences in the electronic structure between the rectangular unit-cell gadolinium thin films and the conventional hexagonal gadolinium films (which is shown in figure 17(b)) are immense. While the dispersion of the state near the Fermi energy (0.3 eV at $\bar{\Gamma}$) for the rectangular Gd film is similar to the Gd(0001) surface state, the other 5d, 6s bands differ from the accepted dispersion behaviour of Gd(0001). The 5d, 6s bulk bands of the rectangular ordered Gd (1.8 eV at $\bar{\Gamma}$) disperse in a direction opposite to the relaxed hexagonal Gd, namely downwards to higher binding energies. Approximately half way through the zone, the bulk bands split into two non-degenerate components which reach a maximum energy separation of approximately 0.8 eV at the zone edge $\bar{X}''$, with the higher binding energy band located at 2.6 eV below E_F (figure 14).

In figure 15 normal incident inverse photoemission spectra (IPES) are combined with

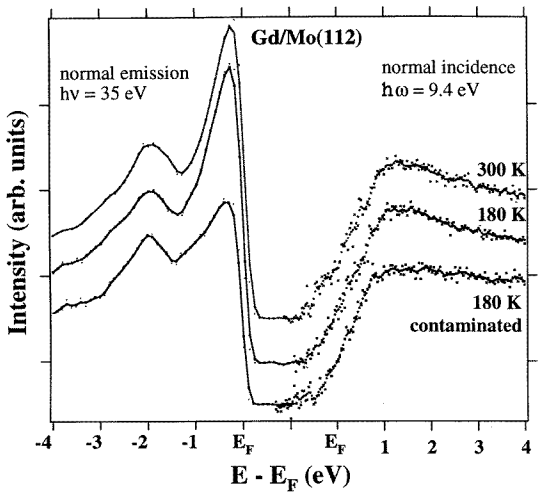

Figure 15. Photoemission (left) and inverse photoemission (right) spectra of an 8 ML thick Gd film grown on Mo(112). The PES spectra were acquired at normal emission with 35 eV photons and the IPES at normal electron incidence in the isochromatic mode, respectively. The spectra were taken for a clean film at 300 K (top), at 180 K (centre), as well as for a slightly contaminated surface at 180 K (bottom).

normal emission PES spectra acquired with 35 eV photons. The three pairs of PES and IPES spectra were obtained under identical conditions, for films at (i) 300 K (top), (ii) 180 K (centre), and (iii) a slightly contaminated film at 180 K (bottom). The two clean PES–IPES spectra manifest an identical band structure at zone centre over the entire temperature range from 180 K to 300 K. Both the occupied and unoccupied bands of the rectangular lattice Gd films demonstrate profound sensitivity to contamination. Small amounts of adsorbates (the exposure of the 'contaminated' film in figure 15 is less than 0.05 L oxygen and/or hydrogen) have large effects on the electronic band structure in the region close to the Fermi level (both occupied and unoccupied). The $5d_{z^2-r^2}$ Gd surface state at 0.3 eV below E_F is dramatically decreased in emission intensity and is shifted towards the Fermi level with small amounts of contamination. Similarly, the unoccupied surface state near the Fermi level decreases and shifts towards E_F with contamination.

The tremendous lattice mismatch of the Mo(112) surface, as well as the strongly interacting Gd interface layer, drives additional thin-film Gd layers into lattice positions that partially relieve the lattice mismatch by adjustments of Gd positions perpendicular to the corrugation direction (⟨110⟩-direction). Along the furrows (⟨111⟩-direction) additional Gd layers follow the structure imprinted by the Gd interface layer. The adjustments perpendicular to the corrugations result in intermediate rectangular ordered thin Gd films, possibly resembling the reconstructed hcp $(10\underline{1}2)$ surface.

6. The electronic structure of strained Gd films

A set of valence-band photoemission spectra of gadolinium films, approximately 150 Å thick, grown on Mo(112), are shown in figure 16 for various points along the $\overline{\Gamma\Sigma M}$ high-symmetry line of the hexagonal surface Brillouin zone. The spectra were acquired with p-polarized light and a photon energy of 38.6 eV at approximately 145 K. The normal

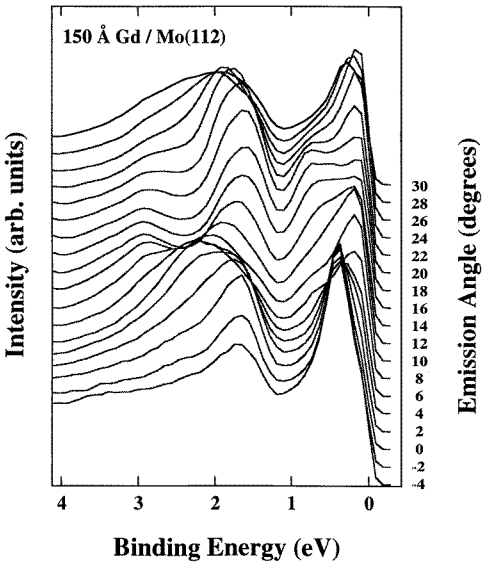

Figure 16. The emission angle dependent photoemission spectra of a 150 Å Gd film grown on Mo(112) along the $\overline{\Gamma\Sigma M}$ high-symmetry direction of the surface Brillouin zone. The spectra were acquired at 145 K with a photon energy of 38.6 eV.

emission spectra are characterized by the Gd 4f core level at 8.4 eV binding energy, the Gd 5d, 6s bulk band at ∼1.6 eV below E_F and the Gd $5d_{z^2-r^2}$ surface state at ∼0.4 eV binding energy, as well as a Gd bulk band near the Fermi level. At normal emission the valence-band spectrum of the strained hexagonal Gd film very closely resembles the photoemission spectrum of ordered Gd films of intermediate thickness with the rectangular SBZ. Similar to the thinner rectangular lattice Gd films, the thicker strained hexagonal lattice Gd film exhibits band dispersions distinct from unstrained Gd(0001) [5, 8, 9]. Near the zone edge $\bar{M}$ the valence band spectra clearly reveal two distinct states near the Fermi level, (i) the $5d_{z^2-r^2}$ surface state at approximately 0.7 eV binding energy and (ii) a Gd 5d, 6s bulk band at or near the Fermi level.

The two-dimensional nature of the $5d_{z^2-r^2}$ Gd surface state of the strained hcp (0001) or fcc (111) Gd films at a binding energy of 0.7 eV is illustrated in figure 17. This figure shows a close up of the valence band of a 150 Å Gd film of the region near the Fermi level for a variety of photon energies. The binding energy of the state approximately 0.7 eV below E_F is invariant under changes of perpendicular momentum (as indicated by the dashed line), which is characteristic of a surface state or surface resonance. The state closest to the Fermi level shifts in binding energy with different photon energies which necessarily assigns this feature to having bulk character.

The electronic valence-band structure along the $\overline{\Gamma\Sigma M}$ high-symmetry line is shown in figure 18(a) for the 150 Å thick strained Gd film and are compared to the band structure of unstrained Gd(0001) (figure 18(b)) [5, 12]. The 5d, 6s bulk bands of the strained hexagonal ordered Gd films disperse in a similar fashion to the bulk bands of the rectangular ordered thin Gd films, but opposite to 'relaxed' unstrained hexagonal Gd(0001). These bands form a broad feature at approximately 1.6 eV binding energy at $\bar{\Gamma}$, which tails towards the higher-binding-energy side. The bulk bands disperse away from E_F to higher binding energies with increasing wave vector. Approximately half way through the zone, the bulk bands

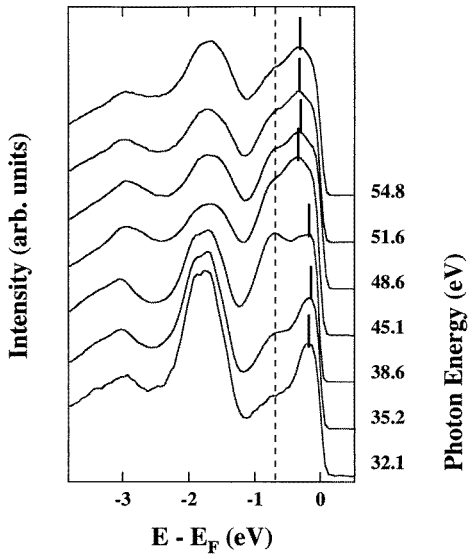

Figure 17. Photoemission spectra of a 150 Å Gd film grown on Mo(112) for various photon energies acquired at 145 K with an electron emission angle of 16 degrees off normal. The dotted line marks the rigid position of a state with surface character while the tick marks indicate the position of a band near the Fermi level with bulk character.

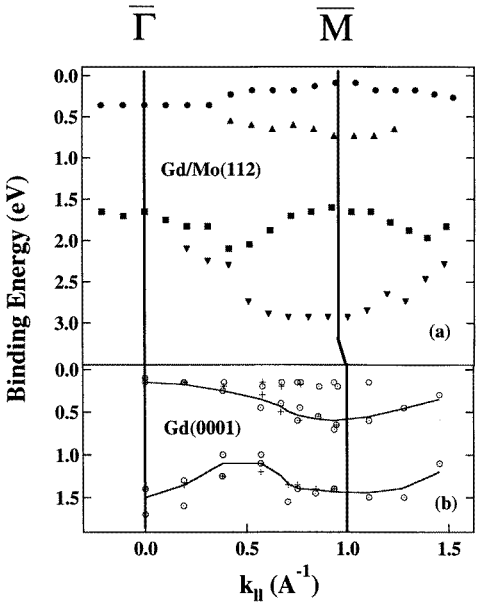

Figure 18. (a) The band dispersion of a strained Gd film along the $\overline{\Gamma\Sigma M}$ high-symmetry direction of the surface Brillouin zone. (b) The experimental band dispersion of an ordered Gd(0001) film grown on W(110) along $\overline{\Gamma\Sigma M}$ of the surface Brillouin zone The data were reduced from [4] and [12].

split into two non-degenerate components which reach a maximum energy separation of approximately 1.3 eV at the zone edge $\bar{M}$, with the higher-binding-energy band located at

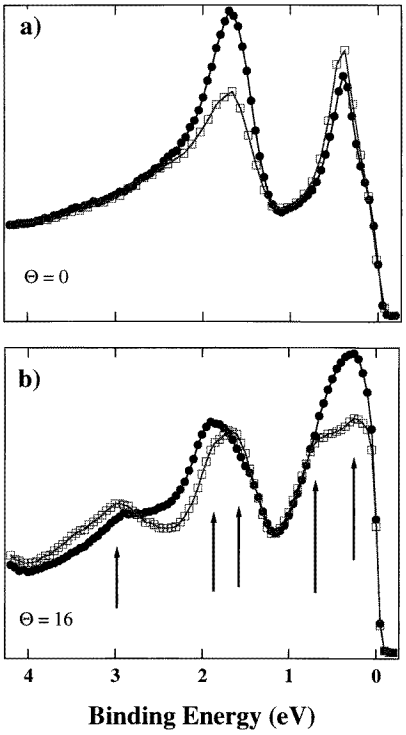

Figure 19. Photoemission spectra of a 150 Å Gd film grown on Mo(112) acquired with s-polarized light (●), and p-polarized light (□) for (a) normal emission and (b) 16 degrees off normal.

2.9 eV below E_F. The surface state of the strained Gd film (0.4 eV at $\bar{\Gamma}$) disperses away from the Fermi level in a manner similar to the Gd(0001) surface state. Nevertheless, the strained surface state appears to be shifted towards higher binding energies by approximately 0.2 eV as compared to the unstrained surface state. In addition, there is a Gd 5d, 6s bulk band that is located near the Fermi level at the zone centre and which disperses towards the Fermi level along the $\overline{\Gamma\Sigma M}$ high-symmetry line of the hexagonal Brillouin zone of the strained hcp (0001) or fcc (111) Gd film.

The strain within the Gd/Mo(112) is clearly reflected in the reduced SBZ size. Based on careful analysis of the LEED and the dispersion of the Gd 5d, 6s bulk bands, the $\bar{M}$ of the strained Gd film was determined to be at $\boldsymbol{k}_{\parallel} = 0.96$ Å^{-1}, which is reduced by approximately 4% as compared to the unstrained Gd(0001) film ($\bar{\Gamma}$–$\bar{M} = 1.0$ Å^{-1}).

7. Symmetry of strained hexagonal lattice Gd states

Dipole selection rules have been invoked to determine the symmetry of the Gd-induced states for both the ultra-thin and thin films of Gd grown on Mo(112) as discussed earlier.

For the thicker strained hcp (0001) or fcc (111) Gd films the symmetry of the bands appears to be different from either the monolayer Gd hexagonal lattice or the moderate-film-thickness (3–10 ML) rectangular lattice. Figure 19(a) shows two normal emission valence-band spectra in s- and p-polarized light for an approximately 150 Å thick Gd film.

The overall symmetry of the hexagonal SBZ of the thicker Gd films is represented by the C_{6v} or C_{3v} symmetry group. At first glance at normal emission the spectra show two bands in the valence band of the strained Gd films, (i) a state at approximately 0.4 eV binding energy with enhanced emission intensity for p-polarized light and (ii) a band centred at 1.8 eV binding energy which is enhanced under s-polarized light. This indicates that the relatively sharp surface state below E_F is of a_1 symmetry (Δ_1 or Δ_2 C_{6v} representations) and predominantly of Gd $5d_{z^2-r^2}$ character similar to the unstrained Gd(0001) surface. The bulk bands at 1.8 eV at first glance appear to be of Δ_5 or Δ_6 symmetry, which favours the possibility of Gd $5d_{xz,yz}$ or Gd $5d_{x^2-y^2}$ character. We cannot determine the symmetry of the bulk character state near E_F from our measurements.

Near the zone edge $\bar{M}$, the lifting of the degeneracy reveals a more complicated picture of the band structure, as seen in figure 19(b). At least five different bands of different symmetry character can be identified, as indicated by the markers. Nevertheless without any complementary information a complete character assignment of these bands at wave vectors near the Brillouin zone edge is not possible, but a strong mixture of Δ_5 or Δ_6 with Δ_1 or Δ_2 is suggested away from $\bar{\Gamma}$.

It is important to note that the Gd–Mo interface state at 0.3 eV binding energy for the ultra-thin film has b_1 symmetry ($5d_{xz}$ character), while the corresponding surface state for the intermediate films has a_1 symmetry ($5d_{z^2-r^2}$ character). This implies that during the growth of the Gd films on Mo(112) the symmetry of the surface state evolves from b_1 to a_1. This is in excellent agreement with our observation that the interface state diminishes for coverages beyond the well ordered 0.7 ML films. The alteration in symmetry of the surface state is illustrated in the bottom panel of figure 20, which shows the relative surface state intensities of the Gd $5d_{xz}$ interface state (acquired with 52 eV photon energy) and the Gd $5d_{z^2-r^2}$ surface state (acquired with 35 eV photon energy). In this figure, we have made use of the resonant photoemission effect [45], and it can be seen that the Gd surface switches symmetry in the coverage region between 1 and 3 monolayers. The switching in symmetry and bonding configuration of the Gd surface is associated with drastic changes in the electron effective mass and interaction strength, which will be discussed in the following section. In a similar fashion the Gd bulk bands at the zone centre switch symmetry from a predominantly a_1 character for the Gd films of intermediate thickness (3–10 ML) to predominantly e_1 or e_2 character for the thicker strained hexagonal films. This is also in agreement with our postulated structural change from reconstructed hcp ($10\underline{1}2$) for the intermediate Gd films to hcp (0001) or fcc (111) for the thicker Gd films.

The effects of the strain of the thicker Gd films is clearly reflected in the reduced Brillouin zone as compared to the unstrained Gd(0001) (figure 17). Although the symmetry of the bulk bands of the strained Gd films are even with respect to the mirror plane at $\bar{\Gamma}$, as is the case for unstrained Gd(0001), the observed mixed symmetry character at the zone edge suggests that the orbital symmetry of these strained Gd 5d, 6s bulk bands may still be different from that of unstrained Gd(0001). The questions concerning the origin of the modified band structure of the strained Gd films, however, remains unanswered. Theoretical band structures, which are lacking at this point, are needed to resolve these issues for strained layers of Gd.

8. The effective mass

The analysis of the dispersion of the interface state at 0.3 eV binding energy at $\bar{\Gamma}$ provides insight into the localization and hybridization of the electron orbitals in the ultra-thin Gd overlayer. A line shape fitting of the interface state dispersion with a parabolic function

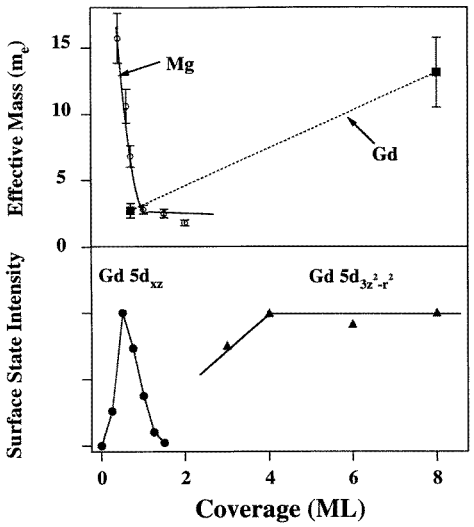

Figure 20. The effective mass of Mg (○) and Gd (■) as a function of film thickness (top panel). The data points for Mg are extracted from [45] and [46]. The bottom panel shows normalized photoelectron emission intensities of the Gd 5d$_{xz}$ interface state (l) and the 5d$_{z^2-r^2}$ surface state (▲) at ∼0.3 eV binding energy at Γ versus Gd coverage (ML). The data points were extracted from the spectra acquired with 52 eV and 35 eV photon energy, respectively.

centred about $\bar{\Gamma}$ was used to determine the electron effective mass m^* of the interface state. The interface state dispersed nearly isotropically along the two perpendicular directions $\overline{\Gamma X'}$ and $\overline{\Gamma Y'}$. This is in agreement with the atomic distances, proposed by our model, which are roughly the same for both directions indicating similar hybridization. The average electron effective mass along both high-symmetry directions, $\overline{\Gamma X'}$ and $\overline{\Gamma Y'}$ was determined as $m^* = (2.7 \pm 0.2)\ m_e$. This is a relatively small value for m^*, which is indicative of a light electron in the Gd interface state. The effective mass is related to the electron correlation energy, and influenced by many-body effects. A light electron is distinctive for a bandlike (delocalized) electronic phase. The effective mass of the Gd interface state describes an almost free-electron-like condition. Since significant wave function overlap between neighbouring Gd atoms is unlikely, the light electron mass furthermore implies a strong interaction of the ultra-thin Gd layer with the Mo(112) substrate. The strong interaction causes the trapping of electrons in a narrowly defined interlayer region.

The relatively small effective mass of the Gd–Mo interface state is exactly opposite to the behaviour observed with ultra-thin films of Mg [46, 47] on Mo(112). Figure 20 shows the effective mass of Mg (○), and Gd (■) plotted as function of overlayer coverage (top panel). The effective mass of ultra-thin films of the Mg interface state is of the order of 15.5 m_e, more than five times larger than the 2.7 m_e of the corresponding Gd overlayer. With increasing film thickness the effective mass for the Mg surface decreases quickly, in contrast to the Gd film, which manifests a gain in effective mass, with a value of $(13.1 \pm 2.0)\ m_e$ for an 8 ML thick film. The implications are seen in the bonding strengths. The interfacial Mg overlayer is weakly bound to the Mo(112) substrate, while Mg intrafilm interactions are quite strong. In the case of Gd the situation is reversed. Gd exhibits strong bonding to the Mo substrate while the surface of a thicker Gd film will experience weaker interaction with the bulk. The explanation for this behaviour can be attributed to the differences in the electron

valency between the two systems ($5d^16s^2$ for Gd and $3s^2$ for Mg). The strong interaction between the substrate and the Gd overlayer is a consequence of the strong hybridization of the Gd $5d_{xz}/6p_x$ and Mo $4d_{xz}/5p_x$ orbitals. The b_1 or b_2 symmetry orbitals are not available for bonding with the fully symmetric Mg s orbitals. Furthermore, as seen in figure 20, the effective mass of the Gd surface state can be correlated with the symmetry of this feature. The Gd $5d_{xz}$ interface state is characterized by a light effective mass while the Gd $5d_{z^2-r^2}$ surface state is identified as a heavy electron state.

The strongly interacting Gd atoms in the Gd–Mo interface layer are locked tightly in lattice positions, which are unfavourable for the additional epitaxial Gd film growth. Even though the interface lattice resembles a uniaxially distorted hexagonal lattice (see figure 3, right panel) the lattice mismatch as compared to the unstrained hcp Gd(0001) is enormous. This incommensurate lattice mismatch and the indication of translationally shifted domains along the ⟨110⟩ direction of the interface layer results in the formation of intermediate Gd films with rectangular SBZ that possibly order in a reconstructed hcp $(10\underline{1}2)$ structure, as well as strained hexagonal films with dislocations for the thicker Gd films (thicknesses of more than approximately 10 ML).

For thicker films the strained hexagonal Gd structure demonstrates the robust nature of growth along the fcc (111) or hcp (0001) direction. This has been observed before [48]. It is important to recognize that the lattice constant of the rectangular Gd film of 3.77 Å is identical to the determined strained lattice constant of the expanded hexagonal structure for the thicker Gd films. Nevertheless, the transition from a rectangular, possibly reconstructed hcp $(10\underline{1}2)$ to a hexagonal hcp (0001) or fcc (111) lattice structure requires significant rearrangement of atoms which is reflected in the streaks that are clearly visible in the LEED pictures. Throughout the film growth the lattice dislocations and misfits occur along the ⟨110⟩ substrate direction.

9. Conclusion

In growing Gd on a corrugated (112) surface of molybdenum we have been able to obtain altered faces of Gd.

Ultra-thin films of 0.7 ML coverage order in a $p(3\times2)$ structure and exhibit an interface state at ∼0.3 eV below E_F and a surface state at 1.8 eV binding energy. The symmetry of the two states were determined as b_1 and a_1, respectively, in the C_{2v} point group. The ultra-thin Gd film is characterized by strong interactions with the Mo(112) substrate, established by the largely hybridizing Gd $5d_{xz}/6p_x$ interface state with the substrate $4d_{z^2-r^2}/5p_x$ orbitals, and the wave function overlap of Gd 6s with the Mo $5p_z$ orbitals. The strong interactions of the interface layer with the substrate is reflected by the light effective mass of $m^* \approx (2.7 \pm 0.2)\ m_e$ of the interface state electrons.

The unfavourable lattice match between the Mo(112) and the hcp Gd lattice, as well as the strongly bonded Gd interface layer results in rectangular ordered and uniaxially dislocated thin Gd films (3–10 ML), which are possibly related to the hcp $(10\underline{1}2)$ orientation. The symmetry of the surface state at 0.3 eV binding energy switches from b_1 (Gd $5d_{xz}/6p_x$ character) to a_1 (Gd $5d_{z^2-r^2}/6s$ character) as the film thickness is increased beyond 1 ML. This is associated with an increase in effective mass by a factor of five, indicating weaker interactions within the Gd film. Misfit dislocations are apparent in the direction perpendicular to the substrate corrugations, as indicated by (i) the absence of band dispersion along the $\overline{\Gamma Y''}$ direction of the SBZ, which reflects the lack in long-range crystallographic order along the ⟨110⟩ direction and (ii) the vertical streaks in the LEED pattern of the rectangular unit-cell gadolinium.

The misfit dislocations are still evident for films much thicker than 10 ML where the Gd films order in a strained hexagonal lattice with a reduced Brillouin zone size of ∼4%. The thicker Gd films grow in a strained hcp (0001) or fcc (111) surface structure which cannot be uniquely determined. As a result of the strain or altered stacking order, the Gd 5d, 6s bulk bands disperse opposite to those of the conventional Gd(0001). At least one band is located at $\bar{\Gamma}$ that disperses to higher binding energies along $\bar{\Gamma}\bar{\Sigma}\bar{M}$, while in the vicinity of the zone edge $\bar{M}$ two bands are observed, separated by a maximum energy splitting of ∼1.3 eV. No temperature dependence has been observed for either the occupied or unoccupied electronic structure of thin strained Gd films at the zone centre over the temperature range from 180 K to 300 K. The occupied and unoccupied surface states near the Fermi level are very sensitive to surface contamination.

Our achievement of growing altered surfaces of Gd opens the door for renewed investigations dedicated towards the understanding of magnetic ordering in rare earth materials where electron localization is an issue. The rigidity in the temperature dependence of the clean surface states at the zone centre in the occupied and unoccupied region of the band structure does not provide much support for Stoner-like behaviour for the surface of thin rectangular ordered Gd films grown on Mo(112). Decreased itinerancy within the altered SBZ is certainly expected to decrease any form of Stoner-like coupling. Strain, even expansive strain is believed to result in continued ferromagnetic ordering [33]. If there is any form of magnetic ordering within these Gd films, it would be interesting to determine if and to what extent the modified face or strain alters the magnetic interactions and how it will effect the correlation of the magnetic moments.

Acknowledgments

This work was supported by NSF through grant No DMR-92-21655, DMR-94-07933 and DMR-94-96131. The experiments were carried out at the Synchrotron Radiation Center which is also funded by NSF. The assistance of T McAvoy in carrying out this work is gratefully acknowledged.

References

[1] Dowben P A, McIlroy D N and Li Dongqi 1997 *Handbook on the Physics and Chemistry of Rare Earths* vol 24, ed K A Schneider and L Eyring (Amsterdam: North-Holland) pp 1–46
[2] Barrett S D 1992 *Surf. Sci. Rep.* **14** 271
[3] Himpsel F J and Reihl B 1983 *Phys. Rev.* B **28** 574
[4] Bongsoo Kim, Andrews A B, Erskine J L, Kim Kwang Joo and Harmon B N 1992 *Phys. Rev. Lett.* **68** 1931
[5] Li Dongqi, Hutchings C W, Dowben P A, Hwang C, Rong-Tzong Wu, Onellion M, Andrews A B and Erskine J L 1991 *J. Magn. Magn. Mater.* **99** 85
[6] Li Dongqi, Jiandi Zhang, Dowben P A, Rong-Tzong Wu, and Onellion M 1992 *J. Phys.: Condens. Matter* **4** 3929
[7] Li Dongqi, Dowben P A, Ortega J E and Himpsel F J 1994 *Phys. Rev.* B **49** 7734
Donath M, Gubanka B and Passek F 1996 *Phys. Rev. Lett.* **77** 5158
[8] Li Dongqi, Pearson J, Bader S D, McIlroy D N, Waldfried C and Dowben P A 1996 *J. Appl. Phys.* **79** 5838
Weschke E, Schussler-Langeheine C, Meier R, Fedarov A V, Starke K, Hübinger F and Kaindel G 1996 *Phys. Rev. Lett.* **77** 3415
[9] Li Dongqi, Pearson J, Bader S D, McIlroy D N, Waldfried C and Dowben P A 1995 *Phys. Rev.* B **51** 13 895
[10] Li Dongqi, Jiandi Zhang, Dowben P A and Onellion M 1993 *Phys. Rev.* B **8** 5612
[11] Li Dongqi, Hutchings C W, Dowben P A, Ron-Tzong Wu, Hwang C, Onellion M, Andrews A B and Erskine J L 1991 *J. Appl. Phys.* **70** 6565
[12] Li Dongqi, Jiandi Zhang, Dowben P A and Onellion M 1992 *Phys. Rev.* B **45** 7272
[13] Nolting W, Borgiel W, Dose V and Fauster Th 1987 *Phys. Rev.* B **35** 7025

[14] Nolting W 1985 *Phys. Rev.* B **32** 403
Nolting W, Bei de Kellen S and Borstel G 1991 *Phys. Rev.* B **43** 1117
[15] Nolting W, Dambeck T and Borstel G 1994 *Z. Phys.* B **94** 409
Nolting W, Borstel G, Dambeck T, Fauster T and Vega A 1995 *J. Magn. Magn. Mater.* **140–144** 55
[16] Harmon B N and Freeman A J 1974 *Phys. Rev.* B **10** 1979
[17] Harmon B A and Freeman A J 1974 *Phys. Rev.* B **10** 4849
[18] Borgiel W, Borstel G and Nolting W 1986 *Solid State Commun.* **60** 313
[19] Borgiel W and Nolting W 1990 *Z. Phys.* B **78** 241
[20] Eriksson O, Ahuja R, Ormeci A, Trygg J, Hjortstam O, Söderlind P, Johansson B and Wills J M 1995 *Phys. Rev.* B **52** 4420
[21] Freeman A J and Ruqian Wu 1991 *J. Magn. Magn. Mater.* **100** 497
Ruquian Wu, Chun Li, Freeman A J and Fu C L 1991 *Phys. Rev.* B **44** 9400
[22] Wu S C, Li H, Li Y S, Tian D, Quinn J, Jona F and Fort D 1991 *Phys. Rev.* B **44** 13 720
[23] Rau C and Robert M 1987 *Phys. Rev. Lett.* **58** 2714
Rau C and Eichner S 1986 *Phys. Rev.* B **34** 6347
[24] Weller D, Alvarado S F, Gudat W, Schroder K and Campagna M 1985 *Phys. Rev. Lett.* **54** 1555
[25] Weller D and Alvarado S F 1988 *Phys. Rev.* B **37** 9911
[26] Tang H, Walker T G, Hopster H, Pappas D P, Weller D and Scott J C 1993 *Phys. Rev.* B **47** 5047
[27] Li Dongqi, Jiandi Zhang, Dowben P A, Garrison K, Johnson P D, Tang H, Walker T G, Hopster H, Scott J C, Weller D and Pappas D P 1993 *Mater. Res. Soc. Symp. Proc.* vol 313 (Pittsburgh, PA: Materials Research Society) p 451
[28] McIlroy D N, Waldfried C, Li Dongqi, Pearson J, Bader S, Huang D-J, Johnson P D, Sabirianov R F, Jaswal S S and Dowben P A 1996 *Phys. Rev. Lett.* **76** 2802
[29] Weller D and Alvarado S F 1986 *J. Appl. Phys.* **59** 2908
[30] Moruzzi V L, Marcus P M, Schwarz K and Mohn P 1986 *Phys. Rev.* B **34** 1784
[31] Dowben P A, Varma S, Kime Y J, Mueller D R and Onellion M 1988 *Z. Phys.* B **73** 247
[32] De S K and Chatterjee S 1987 *J. Phys. F: Met. Phys.* **17** 2057
Dakshinamoorthy M, Iyakutti K, Sankar S and Asokamani R 1984 *Z. Phys.* B **55** 299
De S, Bose I and Chatterjes S 1985 *Phys. Status Solidi* B **127** 605
Glötzel D 1981 *Physics of Solids Under High Pressure* ed J S Schilling and R N Shelton (Amsterdam: North-Holland) p 263
Mcmahan A K, Shriver H L and Johansson B 1981 *Physics of Solids Under High Pressure* ed J S Schilling and R N Shelton (Amsterdam: North-Holland) p 169
[33] Harmon B N, Antropov U P, Liechtenstein A I, Solovyev J V and Anisinov V I 1995 *J. Phys. Chem. Solids* **56** 1521
Eriksson O, Ahuja R, Ormeci A, Tsygg J, Hjorstam O, Sönderlind P, Johansson B and Wills J M 1995 *Phys. Rev.* B **52** 4420
[34] Waldfried C, McIlroy D N, Hutchings C W and Dowben P A 1996 *Phys. Rev.* B **54** 16460 erratum
[35] Erdmann P W and Zipf E C 1982 *Rev. Sci. Instrum.* **53** 235
[36] Pearson W B 1967 *Handbook of Lattice Spacings and Structures of Metals and Alloys* (Oxford: Pergamon)
[37] Du R and Flynn C P 1990 *J. Phys.: Condens. Matter* **2** 1335
[38] Huang J C A, Du R-R and Flynn C P 1991 *Phys. Rev.* B **44** 4060
[39] Hong S C and Freeman A J 1997 *Bull. Amer. Phys. Soc.* **42** 201
[40] Waldfried C, McIlroy D N, Jiandi Zhang, Dowben P A, Katrich G A and Plummer E W 1996 *Surf. Sci.* **363** 296
[41] McAvoy T, Waldfried C, Jiandi Zhang, McIlroy D N and Dowben P A in preparation
[42] Jiandi Zhang, Dowben P A, Li Dongqi and Onellion M 1995 *Surf. Sci.* **329** 177
[43] Waldfried C, McIlroy D N, Li Dongqi, Pearson J, Bader S and Dowben P A 1995 *Surf. Sci.* **341** L1072
[44] Jiandi Zhang, Mei W, McAvoy T, Waldfried C, McIlroy D N and Dowben P A in preperation
[45] Dowben P A, Li D, Jiandi Zhang and Onellion M 1995 *J. Vac. Sci. Technol.* A **13** 1549
[46] Jiandi Zhang, McIlroy D N and Dowben P A 1995 *Phys. Rev.* B **52** 11 380
[47] Jiandi Zhang, McIlroy D N and Dowben P A 1995 *Europhys. Lett.* **29** 469
[48] Dowben P A, LaGraff D, Li Dongqi, Miller A, Zhang L, Dottl L and Onellion M 1991 *Phys. Rev.* B **43** 3171